ACS APPLIED BIO MATERIALS

www.acsabm.org Article

Aligned and Oriented Collagen Nanocomposite Fibers as Substrates to Activate Fibroblasts

Giovanni Spiaggia, Patricia Taladriz-Blanco, Dedy Septiadi, Roberto Diego Ortuso, Aaron Lee, Veronique Trappe, Barbara Rothen-Rutishauser, and Alke Petri-Fink*

Cite This: *ACS Appl. Bio Mater.* 2021, 4, 8316–8324 Read Online

ACCESS | Metrics & More | Article Recommendations | Supporting Information

ABSTRACT: Purified collagen possesses weak mechanical properties, hindering its broad application in tissue engineering. Strategies based on manipulating the hydrogel to induce fiber formation or incorporate nanomaterials have been proposed to overcome this issue. Herein, we use a microfluidic device to fabricate, for the first time, collagen hydrogels with aligned and oriented fibers doped with gold nanoparticles and carbon nanotubes. Results based on rheology, atomic force microscopy, and scanning electron microscopy reveal the formation of aligned and oriented collagen fibers possessing greater rigidity and stiffness on the doped hydrogels in comparison with native collagen. The mechanical properties of the hydrogels increased with the nanomaterial loading percentage and the stiffest formulations were those prepared in the presence of carbon nanotubes. We further evaluate the *in vitro* response of NIH-3T3 fibroblasts to the change in stiffness. The cells were found to be viable on all substrates with directional cell growth observed for the carbon nanotube-doped collagen fibers. No significant differences in the cell area, aspect ratio, and intensification of focal adhesions driven by the increase in stiffness were noted. Nonetheless, fibroblast proliferation and secretion of TGF-β1 were greater on the hydrogels doped with carbon nanotubes. This nanomaterial-collagen composite provides unique features for cell and tissue substrate applications.

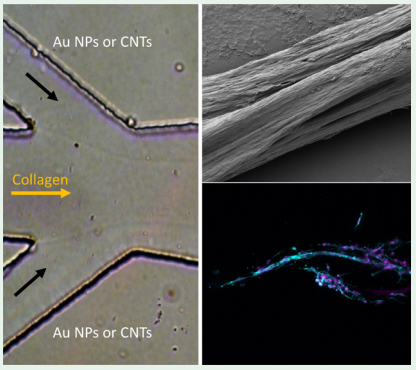

KEYWORDS: *microfluidics, collagen, nanomaterials, fibers alignment, cells*

INTRODUCTION

Collagen is a major constituent and principal structural building block of the native extracellular matrix (ECM) in living tissues. Among the five different types of fibrillar collagens existing in vertebrates (type I, II, III, V, and XI), collagen type I is pre-eminent in tendons, bones, and skin and provides resistance to tensile stresses.[1] Fibrous collagen type I is also present in soft tissues such as the cornea, blood vessels, and heart valves.[2] Therefore, it is not surprising that collagen type I is among the most heavily used proteins in tissue engineering and regenerative medicine, from creating scaffolds for repairing tendon ruptures to healing the skin after an injury.[3]

The alignment (anisotropy) and orientation (directionality) of collagen fibers impact cell behavior as cells respond to the mechanical properties of the ECM that influences cell adhesion, migration, proliferation, morphology, differentiation, and gene expression.[4−6] Biomechanical properties and, in particular, the stiffness of collagen hydrogels have been shown to modify cellular responses, e.g., adhesion and migration through cytoskeletal organization and signaling in adherent cells, such as fibroblasts or epithelial cells.[4,7,8]

Several approaches have been introduced to align collagen fibers *in vitro*[9] such as electrospinning,[10,11] application of external triggers such as magnetic fields,[12] microfluidics,[13−16] and 3D microextrusion printing.[17] Microfluidics has gained great interest in biological research and in the development of new biomaterials as a result of the following: (i) the ability to use very small quantities of samples and reagents, (ii) low cost, (iii) short reaction and analysis times, and (iv) precise control over the flow conditions leading to a homogeneous reaction environment.[18] In simple, the fabrication of collagen fibers in a microfluidic device is driven by shear forces formed inside the device channel when an outer fluid, called shear flow, pushes the inner fluid containing the collagen molecules.[19,20] However, reproducing the biomechanical properties of the native fibril collagen is difficult as the mechanism of *in vivo* fibrillogenesis (i.e., fiber formation) is still not well understood and a high degree of fiber alignment with the appropriate dimensions is difficult to reproduce *in vitro*.[1] Moreover, purified collagen is mechanically weak, which limits its *in vivo* applications.[3]

Received: July 29, 2021
Accepted: November 9, 2021
Published: November 25, 2021

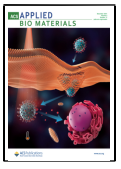

https://doi.org/10.1021/acsabm.1c00844
ACS Appl. Bio Mater. 2021, 4, 8316–8324

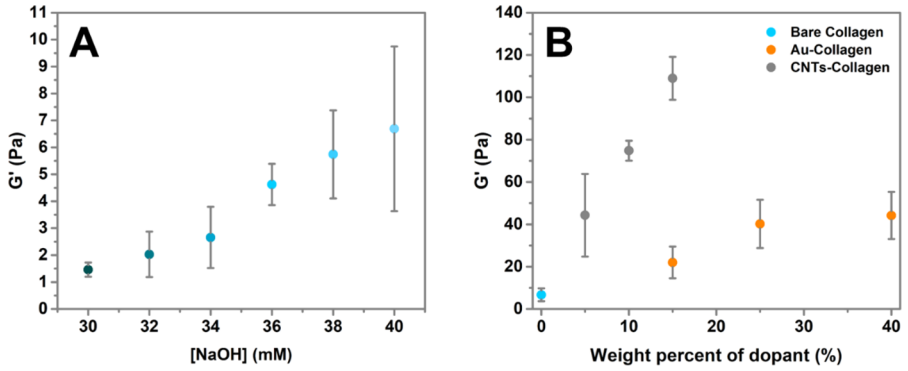

Figure 1. (A) Effect of the NaOH concentration on the storage modulus of collagen hydrogels (n = 3), and (B) the effect of a dopant on the storage modulus of Collagen-40 (n = 3). All experiments were carried out at room temperature.

The use of gold nanoparticles (Au NPs) or carbon nanotubes (CNTs) to reinforce collagen hydrogels by increasing their mechanical properties is a strategy that has been attempted before.[21,22] Homenick *et al.*[23] successfully prepared cast collagen hydrogels with single-walled carbon nanotubes (SWCNTs) by functionalizing the surface of CNTs with poly(ethyleneimine) (PEI), resulting in a nine-fold increase in Young's modulus compared to non-cross-linked hydrogels. Similarly, Kim *et al.*[24] increased the stiffness of collagen fibers by introducing SWCNTs in the collagen matrix to study stem cell differentiation and Xing *et al.*[25] prepared an injectable Au NPs-collagen hydrogel with improved mechanical properties. The hydrogels, prepared by *in situ* reduction of $HAuCl_4$ previously dissolved in the collagen matrix, turned stronger along with the formation of Au NPs.

In this work, we fabricated for the first time collagen hydrogels doped with Au NPs or CNTs in a microfluidic device. The resulting hydrogels, with oriented and aligned fibers, showed 7- and 16-fold increases in stiffness for Au NPs and CNTs-doped collagen hydrogels, respectively. The doped hydrogels were biocompatible and used to evaluate the adhesion, spreading, orientation, proliferation, and differentiation of NIH-3T3 fibroblasts. Our results show that there was no influence on NIH-3T3 morphology compared to aligned and oriented bare collagen fibers. Nonetheless, there was an increase in cell proliferation and fibroblast differentiation on the stiffest doped fibers. The fabricated hydrogels with mechanical properties in the Pascal (Pa) range are potential candidates for the replacement of lung and brain tissues ($G' \approx 100$ Pa[26]).

RESULTS AND DISCUSSION

Rheological Properties of Collagen Hydrogels. Prior to the fabrication and characterization of aligned and oriented fibers, we investigated the effect of NaOH (cross-linking agent) on the mechanical properties of collagen hydrogels in oscillatory strain experiments. Aiming to maximize the stability of the collagen assemblies, we chose to study the effect of NaOH in the range of 30 to 40 mM (see the Experimental Section for more details about the sample preparation). Concentrations of NaOH above 40 mM were not considered as the storage modulus G' of the hydrogels starts to decrease again beyond this concentration (data not shown).

For all hydrogels, the storage modulus G' dominates over the loss modulus G'' (Figure S1), clearly denoting the predominantly solid-like characteristics of these systems. As shown in Figure 1A, the elasticity of the hydrogels increases with the increasing NaOH concentration within the range of NaOH concentrations investigated.

To study the effect of doping the hydrogels with Au NPs or CNTs, we chose to work with the collagen hydrogel obtained 40 mM NaOH, which is the stiffest possible system (Collagen-40, $G'_{\text{Collagen-40}} = 6.7 \pm 3.1$ Pa). The reinforcing effect was evaluated for three concentrations of Au NPs, 15, 25, and 40 wt %, and three concentrations of CNTs, 5, 10, and 15 wt.%, respectively (Figure 1B and Figure S1). The presence of both Au NPs and CNTs leads to an increase of stiffness compared to bare collagen, reaching G' values of 44 ± 11 and 109 ± 10 Pa in the presence of 40 wt % Au (40Au-Collagen) and 15 wt % of CNTs (15CNTs-Collagen), respectively (Figure 1B).

Due to the in-plane shear experiments designed for the mechanical characterization of the collagen hydrogels and the sample symmetry with the rheometer axis of rotation, fiber alignment and orientation does not influence the in-shear hydrogel properties; thus, all the mechanical measurements obtained for the isotropic hydrogels (i.e., non-aligned fibers) can be then adapted to the aligned hydrogels.[27]

Orientation and Alignment of Collagen Fibers. 40Au-Collagen and 15Au-Collagen hydrogels with aligned and oriented fibers were fabricated using the microfluidic device represented in Figure 2. As previously reported in the literature, the mechanical shear force applied in the device induces the alignment of collagen fibers along the direction of the flow.[13−15] The doped-collagen hydrogels were prepared by dispersing either 15 nm Au NPs or CNTs in the collagen solution before introducing them into the microfluidic device (see Figure S2 for details about the characterization of the nanomaterials). For comparison, bare collagen hydrogels fabricated in the same device and cast collagen hydrogels were also prepared. Fiber alignment and orientation can be observed in the SEM pictures shown in Figure 2. In contrast, cast collagen hydrogels exhibited non-aligned fibers due to the absence of shear force and physical constraint (Figure 2).

It has been reported in the literature that collagen fiber formation is highly dependent on the pH or ionic strength of the buffer as helix formation is driven by electrostatic interactions along the collagen fibrils.[1] Changes in these same parameters also alter the mechanical characteristics of the hydrogel, such as its stiffness. When preparing collagen hydrogels in a microfluidic device, changes in channel dimensions or the flow rate impact the fiber morphology, i.e., diameter, width, and length, as well as fiber orientation and alignment.[13,14] In our study, channel dimensions, the flow rate, cross-linking, and collagen concentration were kept constant

https://doi.org/10.1021/acsabm.1c00844
ACS Appl. Bio Mater. 2021, 4, 8316−8324

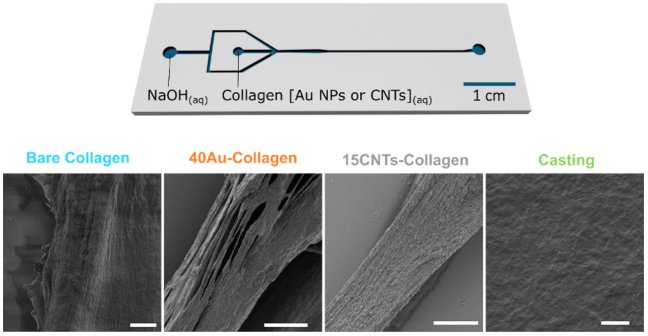

Figure 2. Top row: Schematic representation of the microfluidic device used to align and orient collagen fibers indicating the solutions injected in each of the inlets. Bottom row: SEM pictures of bare collagen, doped collagen hydrogels with 40 wt % Au (40Au-Collagen) and 15 wt % CNTs (15CNTs-Collagen), and cast collagen. The hydrogels were prepared in the microfluidic device using a 3 mg/mL collagen solution and cross-linked with a 40 mM NaOH solution. Au NPs and CNTs were dispersed in the collagen solution before injection into the device. The cast collagen hydrogel was prepared by casting a 3 mg/mL collagen solution cross-linked with a 40 mM NaOH solution with a volume ratio of 1:1. All the experiments were carried out at room temperature. Scale bar: 20 μm.

for all the experiments (see the Experimental Section for more details). Under our experimental conditions, the diameters of the fibers measured from the SEM images were 201 ± 102, 192 ± 63, 236 ± 132 μm for bare, 40Au-Collagen, and 15CNTs-Collagen, respectively.

The alignment of collagen fibers and the presence of Au NPs or CNTs in 40Au-Collagen and 15Au-Collagen were evaluated by AFM and Cytoviva (Figure 3). AFM topography images show oriented collagen fibers for all the investigated hydrogels prepared in microfluidics compared to those observed in the cast collagen. The height channel and relative amplitude channel images show a non-preferential direction of the collagen fibers in the cast collagen compared to the observed in gels prepared using the microfluidic device represented in Figure 2. Similarly, a change in tip amplitude oscillations highlights the presence of fibers in the hydrogels, as reflected in the amplitude channel (Figure 3, bare collagen, white arrows).

The presence of Au NPs in the 40Au-Collagen sample was confirmed by geometrical analysis of the features revealed by the amplitude channel.[28] The different tip-Au NPs interactions compared to those between the tip and the collagen cause changes of oscillation and resonance frequency compared to those produced by the free-standing AFM tip,[29] highlighting the local details in the sample (see Figure S3 and the materials and methods section for more details). Through these datasets, the shape of the projection can be extracted, leading to the identification of the Au NPs within the collagen matrix (Figure 3, left and middle column, second row, and Figure S3). In 40Au-Collagen hydrogels, the NPs were observed as circular areas in which the sizes are consistent with the core diameter of the NPs (data not shown). Similarly, the presence of CNTs in the collagen matrix was determined. It has been reported that CNTs can be identified when embedded in soft matrixes through the analysis of the tip−sample interactions and, in particular, the observation and analysis of the phase image[30] due to the loss of detail resulting from the atomic structure of the carbon-based materials.[31] Therefore, by analyzing the change of tip−sample interaction for 15CNTs-Collagen, the presence of CNTs within the matrix was revealed (Figure 3, third column and Figure S3).

The presence of Au NPs or CNTs within the collagen fibers and its orientation can be clearly seen by Cytoviva due to the scattering properties of these nanomaterials (Figure 3, third column).

Effect of Doping Collagen Fibers on Cell Behavior. In order to investigate the biocompatibility profile and the effect of doping oriented and aligned collagen fibers on cell spreading, i.e., cell size (area) and shape, *in vitro* experiments using NIH-3T3 fibroblasts were performed. No cytotoxicity was observed for all conditions (Figure 4), confirming that the hydrogel alignment and the presence of Au NPs or CNTs does not induce any cytotoxic effect. Fibroblasts were cultured on 40Au-Collagen, 15CNTs-Collagen, and bare collagen hydrogels, respectively (Figure 5), while cast collagen was used as a control.

Confocal laser scanning microscopy (cLSM) and quantitative image analysis were used to visualize and quantify cell morphology and the cell spreading area. At 24 h, cells cultured on bare collagen exhibited the largest area (2067 ± 842 μm^2) followed by 40Au-Collagen (1246 ± 582 μm^2) and 15CNTs-Collagen (1145 ± 359 μm^2), with values closer to those obtained in cast collagen (1215 ± 859 μm^2). At 48 h, the cell area is similar between the cast, bare, and doped collagen hydrogels. There is no difference in the cell area between cells cultured on cast collagen at 24 and 48 h (Figure 5). Cytoskeleton asymmetry was also evaluated by approximating the threshold area to an ellipsoid and dividing the major axis by the minor axis of each signal to obtain the cell aspect ratio (Figure 5). The narrower the cells, the higher the aspect ratio (AR), corresponding to greater asymmetry. NIH-3T3 fibroblasts showed a greater AR on aligned collagen gels at both time points, 24 and 48 h. At 24 h, the highest value was found for 40Au-Collagen (7.19 ± 3.9), while at 48 h, the narrower cells were those cultured on 15CNTs-Collagen (7.83 ± 3.3). As visualized by the cLSM (Figure 5 and Figure S4), SEM images (Figure S4) confirmed that fibroblasts are narrow toward the direction of fiber alignment, while they are more rounded in cast hydrogels.

As abovementioned, channel dimensions, the flow rate, cross-linking, and collagen concentration were kept constant for all the experiments. Therefore, the directional cell growth, cell spreading area, elongation along the fibers, cell proliferation, differentiation, and cell adhesion resulted from culturing NIH-3T3 fibroblast on the doped hydrogels can only be attributed to changes in the hydrogel stiffness induced by the presence of Au NPs or CNTs within the collagen fibers.

Based on our data, hydrogel stiffness caused by the presence of Au or CNTs has no influence on the cell spreading area. The latter is also not strongly influenced by the alignment of the collagen fibers. It is well known that cell spreading on a surface depends on the rigidity of the material where they are cultured. In general, in 2D cultures, the more rigid the material is, the greater the degree of spreading.[32−34] However, the change of stiffness in our formulations was insufficient to induce any change in cell size. The AR of the fibroblast was affected by the alignment of fibers in contrast with the cast collagen hydrogels, inducing directional cell growth. However, the 7- and 16-fold increases in stiffness of 40Au-Collagen and 15CNTs-Collagen seemed to have no effect on cell elongation, signifying that neither Au NPs nor CNTs disrupt fiber alignment.

https://doi.org/10.1021/acsabm.1c00844
ACS Appl. Bio Mater. 2021, 4, 8316−8324

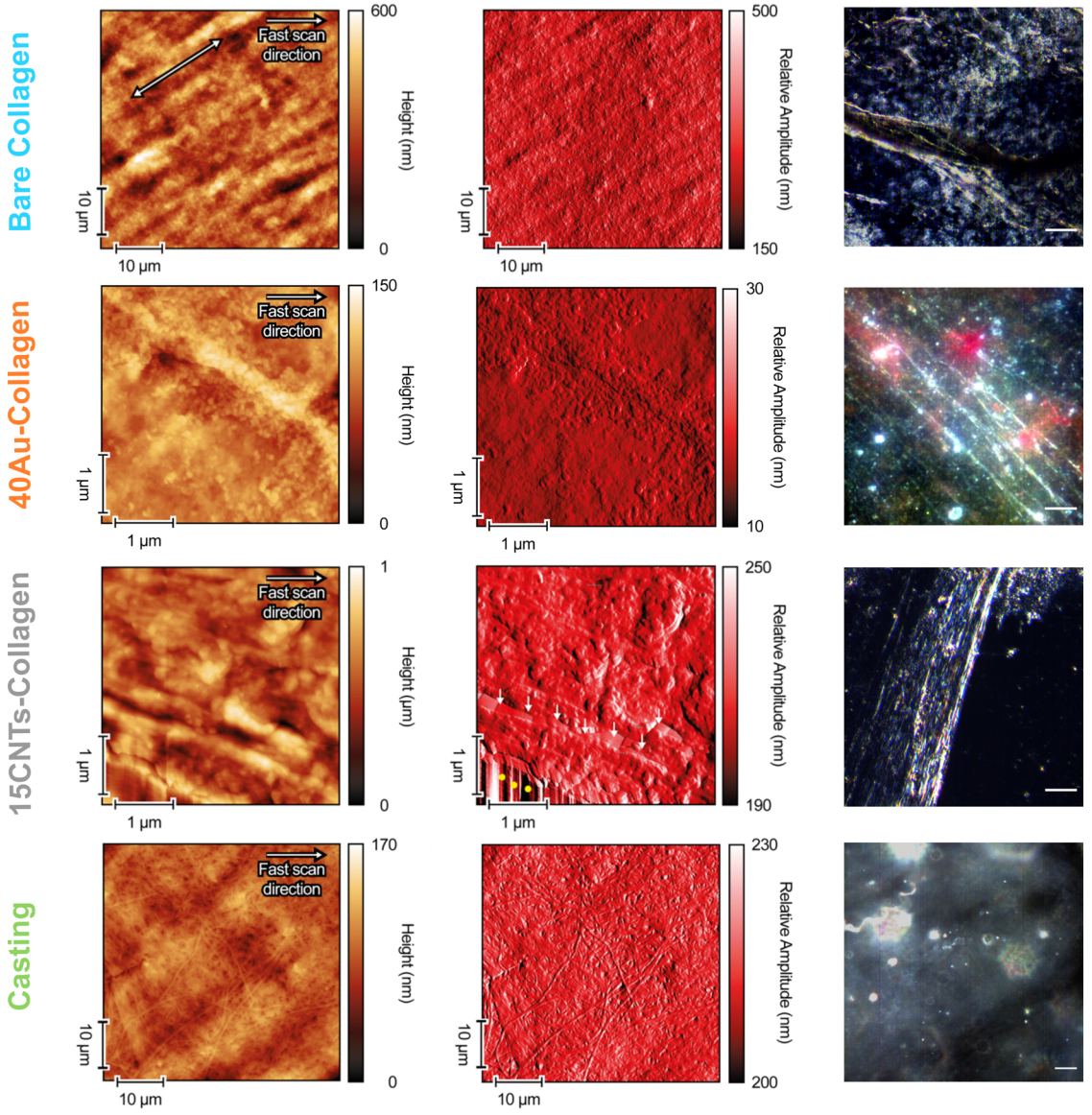

Figure 3. Left and middle columns: AFM topography images of bare collagen (first row, white arrow indicating the direction of the collagen fiber), Au-collagen (second row, 40Au-Collagen), CNTs-doped collagen (third row, 15CNTs-Collagen), and cast collagen (fourth row). The yellow points in the AFM topography image of 15CNTs-Collagen highlight artifacts due to tip−sample interactions. The height of the sample in the highlighted region does not cause a tip−apex interaction, rather a tip−side interaction, and this results in a region of image artifact. The white arrows highlight the presence of CNTs within the collagen fibers. Right column: Cytoviva images of bare collagen (first row), Au-collagen (second row, 40Au-Collagen), CNTs-doped collagen (third row, 15CNTs-Collagen), cast collagen (fourth row), confirming the presence of Au and CNTs within the collagen fibers and its orientation. Scale bar: 10 μm.

Cell proliferation of the fabricated hydrogels was assessed by manually and automatically counting the number of the cells (Figure 6A,B). Both methods show higher cell proliferation for all hydrogels at 48 h and an increase of cell number in the doped collagen fibers compared to cast collagen hydrogels at 24 and 48 h. The highest proliferation was observed in 15CNTs-Collagen at 48 h. This result suggests that the greater rigidity of the collagen fibers caused by the presence of CNTs induces cell proliferation. This behavior was also observed for other 2D substrates where the stiffest formulation leads to higher proliferation rates.[34] However, significant differences were only obtained by manual counting at 24 and 48 h of cultivation (Figure 6A).

The differentiation of fibroblasts into myofibroblasts was evaluated by quantifying the levels of transforming growth factor beta 1 (TGF-β1) released by the fibroblasts (Figure 6C).[35,36] Interferon gamma (IFN-γ) was used as a positive control because of its involvement in the upregulation of TGF-β1 in dermal and corneal fibroblasts.[37] At 24 and 48 h, TGF-β1 secretion by fibroblasts cultured on aligned and oriented collagen fibers expressed secretion levels close to the positive control. Significantly higher concentrations of TGF-β1 were released by cells cultured on all hydrogels with aligned and oriented fibers at 24 h. In particular, cells cultured on 15CNTs-collagen, which present the highest stiffness, secreted the highest amount of TGF-β1. The greater fibroblast proliferation and TGF-β1 secretion on the stiffest hydrogels are consistent with the data reported in the literature.[38,39] Nonetheless, as the secretion of TGF-β1 greatly influences the cellular proliferation rate,[40] TGF-β1 values were normalized by the number of cells

https://doi.org/10.1021/acsabm.1c00844
ACS Appl. Bio Mater. 2021, 4, 8316−8324

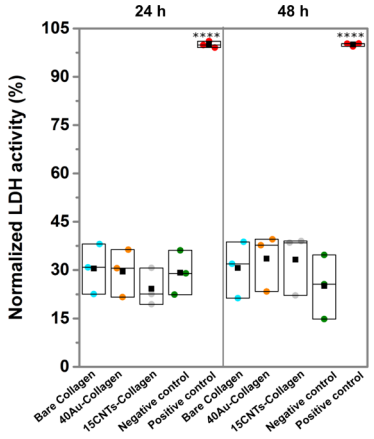

Figure 4. Lactate dehydrogenase assay performed for cells seeded on the collagen hydrogels (2500 cells/mm^2) at 24 and 48 h. Aligned bare collagen (blue dots), aligned Au-doped collagen (40Au-Collagen, orange dots), aligned CNTs-doped collagen (15CNTs-Collagen, grey dots), and cast collagen hydrogels (green dots). Triton X-100 (0.2 vol %) was used as a positive control (red dots). One-way ANOVA with Tukey's multiple test comparison was performed for assessing statistical significance, ****$p \leq 0.0001$. Mean values are represented as black squares (n = 3).

revealing that fibroblasts cultured on the microfluidic fabricated samples exhibited a similar secretion behavior to those cultured on cast collagen (Figure S6). An identical observation was reported by Kievit *et al.*[41] on glioblastoma cells cultured in aligned chitosan−polycaprolactone nanofibers.

Lastly, traction forces exerted by the cells toward the collagen hydrogels were evaluated by the maturation of focal adhesions through visualization of paxillin (Figure S5). In general, larger focal adhesion sizes are associated with stronger cellular adhesion.[42] Based on our observations, the stiffness of the hydrogels induced by the presence of Au and CNTs in the oriented and aligned fibers was not high enough to intensify the localization of focal adhesions at the end of the F-actin.

CONCLUSIONS

In this study, we used microfluidics to fabricate aligned Au- and CNTs-doped collagen fibers that showed greater rigidity than bare aligned collagen with CNTs-collagen being the stiffest formulation. None of the doped hydrogels showed any sign of cytotoxicity, therefore being biocompatible and useful as cell substrates. The size and shape of NIH-3T3 fibroblasts cultured on the hydrogels showed directional cell growth driven by the alignment of the collagen fibers, with no impact of both Au NPs and CNTs on the cell size and aspect ratio. Fibroblast proliferation and release of TGF-β1 were also assessed, revealing an increased cell number and secretion of TGF-β1 on collagen fibers doped with CNTs. After normalization of the TGF-β1 values, no differences in secretion were observed between microfluidic fabricated or cast hydrogels. No effect of the focal adhesion was detected, suggesting that the higher stiffness induced by the presence of the nanomaterials was not high enough to induce it.

EXPERIMENTAL SECTION

Materials. Gibco collagen type I extracted from rat tail with a concentration of 3 mg/mL (solubilized in 20 mM of acetic acid), Invitrogen Alexa Fluor 488 phalloidin, 4′,6-diamidino-2-phenylindole dihydrochloride (DAPI), phosphate-buffered saline (PBS-1X) tablets, and goat anti-rabbit secondary antibody Alexa Fluor 647 were purchased from ThermoFisher Scientific (US). Sodium hydroxide (NaOH, ACS reagent, ≥97.0%), glutaraldehyde solution (50 wt % in H_2O), paraformaldehyde (reagent grade, crystalline), Hellmanex III, hexamethyldisilazane (HMDS, ACS reagent, ≥97.0%), a cytotoxicity detection kit for lactate dehydrogenase (catalyst, diaphorase/NAD^+ mixture, and dye Solution INT and sodium lactate), gold(III) chloride trihydrate ($HAuCl_4{\cdot}3H_2O$, ≥99.9%), and sodium citrate tribasic dihydrate ($C_6H_5Na_3O_7{\cdot}2H_2O$, ≥98%) were obtained from Sigma-Aldrich (Germany). Sylgard 184 silicone elastomer base, poly(dimethylsiloxane) (PDMS, Sylgard 184), and the curing agent were provided by Dow Europe (Switzerland). Nanocyl-7000 MWCNTs were obtained from the European Commission Joint Research Centre, ISPRA, Italy (originated from Nanocyl S.A., Sambreville, Belgium) and used without any further purification. Dulbecco's Modified Eagle Medium (DMEM, ATCC^R 0−2002), penicillin/streptomycin solution (ATCC 30−2300), calf bovine serum (CBS), iron fortified (ATCC^R 30−2030), and L-glutamine solution (200 mM, ATCC^R 30−2214) were acquired from ATCC^R (US). The rabbit monoclonal anti-Paxilin antibody was purchased from Abcam (U.K.). Milli-Q (Merck, Germany) water was used for all the preparations.

Preparation of Casted Gels. Collagen gels were prepared by mixing 300 μL of a 3 mg/mL collagen stock solution with 300 μL of a series of 30, 32, 34, 36, 38, and 40 mM NaOH aqueous solutions, namely, Collagen-30, Collagen-32, Collagen-34, Collagen-36, Collagen-38, and Collagen-40, respectively. The mixture was cast on glass-bottom dishes (glass diameter of 10 mm, MatTek, USA), which were previously cleaned with a 2 vol % solution of Helmanex III in water for 15 min, then subjected to oxygen (O_2 flow = 0.4 atm) plasma (low-pressure Zepto plasma coater, Diener Electronics, Germany) for 1 min. The cast collagen solutions were left undisturbed for 30 min and stored at 4 °C overnight before cell culture experiments.

Synthesis of Au Citrate Nanoparticles (Au NPs). Au NPs were prepared by the well-known Turkevich method.[43] $HAuCl_4$ (0.5 mM) was boiled in the presence of 1.5 mM sodium citrate for 15 min. The solution was cooled down at room temperature and stored in the fridge until use.

Preparation of the Collagen Gels in the Microfluidic Device. Two Omnifix-F syringes (volume = 1 mL, Braun, Switzerland) were filled with solutions of NaOH (outer inlet A, 30 and 40 mM) and collagen (inner inlet B, 3 mg/mL), respectively, and connected to the microfluidic device using PE tubes (inner diameter: 0.38 mm; outer diameter = 1.09 mm, A. Hartenstein, Germany). Both solutions, collagen and NaOH, were pumped into the microfluidic channels using New Era programmable syringe pumps (New Era Pump Systems, Inc., US) at a flow rate of 8.5 μL/min for both inlets. Collagen hydrogels were collected by placing the outlet PE tube toward cleaned glass-bottom dishes for 35 min. Microfluidic gels were left undisturbed for 30 min and stored at 4 °C overnight before cell culture experiments. Au-Collagen and CNTs-Collagen hydrogels were prepared in the same microfluidic device under the same conditions. Au NPs (15, 25, and 40 wt % with respect to collagen weight) and CNTs (5, 10, and 15 wt % with respect to collagen weight) were dispersed in the collagen solution before injection into the device.

Fibroblasts (NIH-3T3) Culture on the Cast and Microfluidic Fabricated Gels. Mouse fibroblasts NIH-3T3 (ATCC^R CRL-1658, US) were cultivated in DMEM supplemented with 10 vol % CBS, 1 vol % penicillin/streptomycin, and 1 vol % of L-glutamine (cDMEM). NIH-3T3 was cultivated in a T75 flask obtained from TPP (Switzerland) at 37 °C, relative humidity of 95%, and CO_2 of 5% until reaching 80% confluency. Cells were washed with PBS (10 mL) and trypsinized with 1.5 mL of trypsin for 5 min. Three milliliters of cDMEM was added and cells were counted using an automatic cell counter (EVE, US). Approximately 120.000 cells were seeded on collagen hydrogels (1500 cell/mm^2) and 1.2 mL of cDMEM was added. Cells were incubated at the incubator for 24 and 48 h, respectively.

Lactate Dehydrogenase (LDH) Assay. Cellular viability was assessed by measuring the release of lactate dehydrogenase into the

https://doi.org/10.1021/acsabm.1c00844
ACS Appl. Bio Mater. 2021, 4, 8316−8324

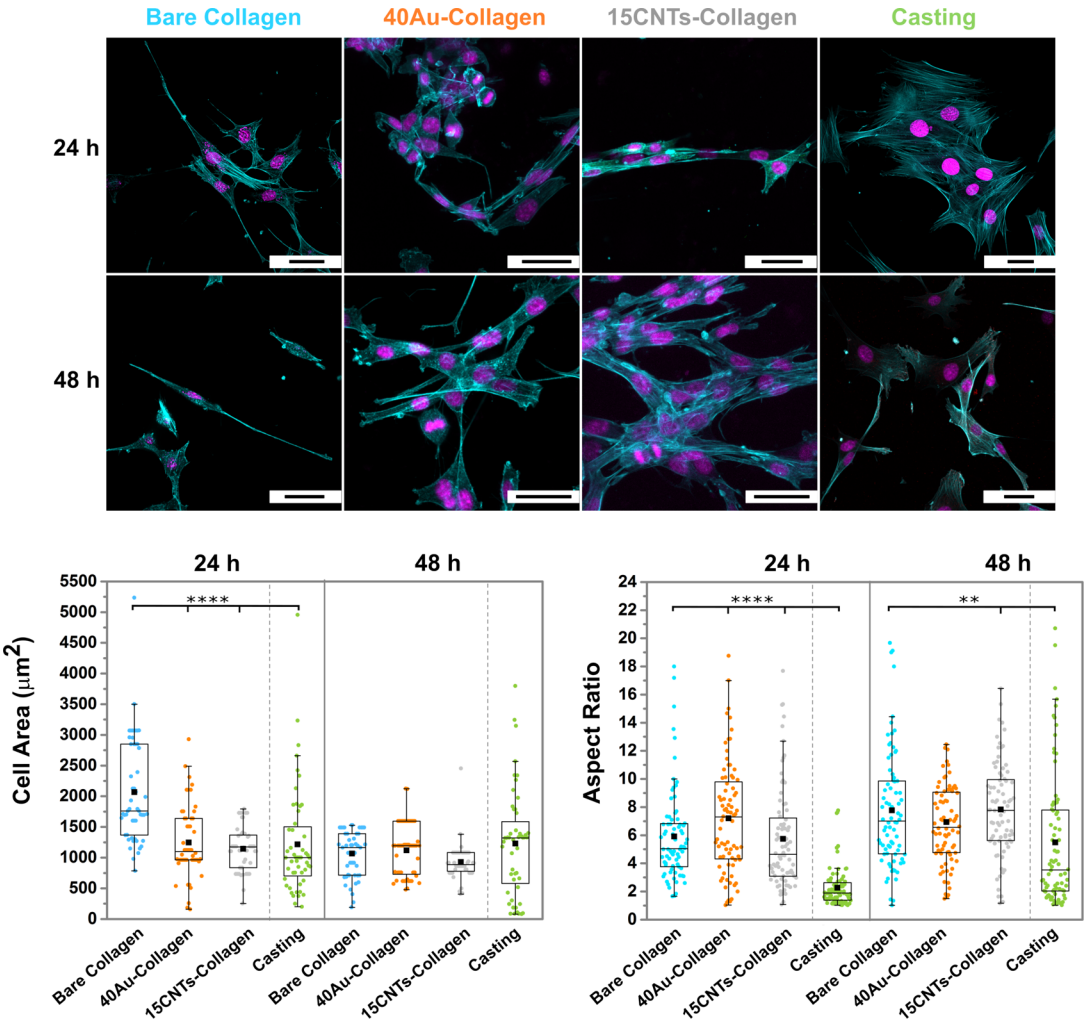

Figure 5. Top row: cLSM images of NIH-3T3 fibroblast cultured on the collagen gels for 24 and 48 h. Number of cells: 1500 cells/mm^2. Cell nuclei (magenta) and F-actin (cyan) were stained with DAPI and Alexa 488 Phalloidin, respectively. Scale bar: 40 μm. Bottom row: area occupied by cells (right, n = 50) and the cellular cytoskeleton aspect ratio (left, n = 80) on the collagen gels after 24 and 48 h. Aligned bare collagen (blue dots), aligned Au-collagen (40Au-Collagen, orange dots), aligned CNTs-doped collagen (15CNTs-Collagen, grey dots), and cast collagen (green dots). Aligned collagen was prepared by injecting a 3 mg/mL solution of collagen and a 40 mM NaOH solution in the microfluidic device represented in Figure 1. Au NPs and CNTs were dispersed in the collagen solution before being injected into the microfluidic device. The cast collagen hydrogel was prepared by casting a 3 mg/mL collagen solution cross-linked with a 40 mM NaOH solution with a volume ratio of 1:1. Mean values are represented as black squares. One-way ANOVA with Tukey's multiple test comparison was performed for assessing the statistical significance, $^{**}p \leq 0.01$ and $^{****}p \leq 0.0001$.

supernatant as a result of cell membrane rupture using an LDH cytotoxicity detection kit (Roche Applied Science, Mannheim, Germany), at 24 and 48 h of cultivation. NIH-3T3 (2500 cells/mm^2) were cultured on 5 gels and 10 other wells that were used as positive (n = 5) and negative controls (100 μL of 0.2 v/v % Triton X-100 in PBS) (n = 5) for the LDH assay. The next day, 100 μL of aliquots of each sample and 100 μL of the LDH assay kit were placed in a new 96-well plate. The absorbance at 630 nm of each sample was measured using a Bio-Rad Plate reader (Switzerland). The data of each measurement was normalized by the mean of the positive control's values.

Profibrotic Response. Transforming growth factor-β1 (TGF-β1) released into the supernatants by the cells was quantified using the respective mouse ELISA DuoSet development diagnostic kit at 24 and 48 h, respectively. Recombinant mouse interferon gamma (1 μg/mL) in cDMEM was used as a positive control.

Fabrication of the Microfluidic Device. The microfluidic chip designed in AUTOCAD 2017 was directly patterned onto a silicon master mold using a SiO_2 hard mask for the silicon dry etching process. A 1 μm-thick plasma-enhanced chemical vapor deposition (PECVD) SiO_2 layer was deposited on a single-side polished (1 0 0) 200 mm Si wafer using a CVD system (MPX from SPTS, UK). The wafer was exposed to HMDS vapor prime to improve the adhesion of the photoresist to the sample, obtained by spin coating of 1.2 μm of AZP4110 (Microchemicals GmbH, Germany) on an SÜSS MicroTec optical track (SÜSS MicroTec AG, Germany). Direct write laser (DWL 2000 Heidelberg Instruments, Switzerland) was used to pattern the photoresist. Following the post bake, the exposed photoresist was developed with AZ400K (Microchemicals GmbH, Germany), and the wafer was rinsed with deionized water and dried. Etching of SiO_2 was completed on a reactive ion etching (RIE) tool (APS from SPTS, UK) with C_4F_8 etching chemistry followed by removal of the photoresist, stripped with an oxygen plasma (PVA GIGAbatch 360 M from Tepla, Germany). The silicon wafer was then etched by a dry etching process performed on an inductively coupled plasma (ICP)-RIE tool (Pegasus from SPTS, UK), using SF_6/C_4F_8 plasma, to transfer the SiO_2 mask features to the bulk silicon. The top remaining SiO_2 mask was then removed. Trench depth was measured using a surface profilometer (KLA-Tencor P-16 Surface Profiler) until

https://doi.org/10.1021/acsabm.1c00844
ACS Appl. Bio Mater. 2021, 4, 8316−8324

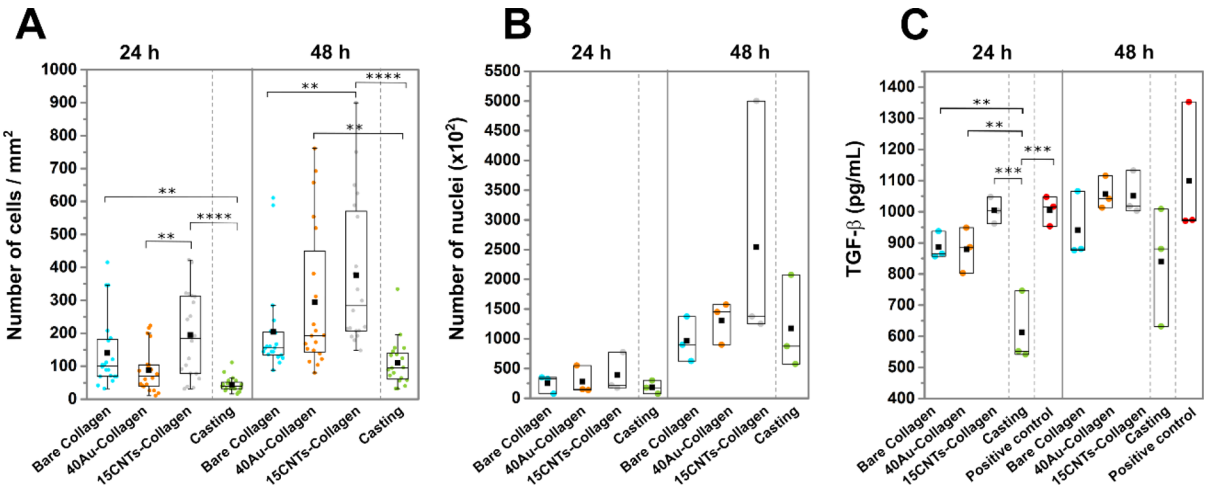

Figure 6. (A) Number of NIH-3T3 fibroblast by manual counting (n = 150) and (B) automatic counting using an EVE counter (n = 3) on the gels after being cultured for 24 and 48 h. (C) Fibrotic response of NIH-3T3 fibroblasts (n = 3) evaluated by measuring the secretion of TGF-β after 24 and 48 h (3625 cells/nm^2). Interferon-gamma (1 μg/mL) was used as a positive control (red dots). One-way ANOVA with Tukey's multiple comparisons test for significance, $^{**}p \leq 0.01$, $^{***}p \leq 0.001$, and $^{****}p \leq 0.0001$. Mean values are represented as black squares.

the desired depth of 75 μm was reached. The dimensions of the device are detailed in Figure S7.

Rheology Measurements. The mechanical characterization of freshly prepared cast collagen hydrogels was performed at 25 °C with an Anton Paar rheometer (MCR 502) equipped with a 50 mm cone and plate geometry (cone angle of 1°) and a solvent trap. The following tests were performed to fully characterize the hydrogels: (i) frequency sweeps, to determine the frequency dependence of the loss and storage moduli in the linear range using a strain of 1% and probing a frequency range from 30 to 1 rad/s, and (ii) amplitude sweeps, to assess the linear viscoelastic range of the sample and the breaking points using a fixed angular frequency of 10 rad/s and increasing the strain logarithmically from 1 to 100%. All measurements were performed three times.

Scanning Electron Microscopy (SEM) Characterization. The surface topography of the hydrogels and the cellular interaction with the cast and microfluidic fabricated hydrogels were evaluated using SEM (TESCAN Mira 3 LM field emission, Czech Republic). Briefly, samples were fixed using a cold aqueous solution of glutaraldehyde (2.5 vol %) for 1 h, washed with Milli-Q water three times and dehydrated by a series of alcohol washes (20, 40, 60, 80, and 100 vol % ethanol) for 5 min each and treated with a solution of HMDS in ethanol (volume ratio of 1:1). Samples were left to dry overnight and sputter-coated (Sputter Coater 108 Auto, Cressington Scientific Instruments) with 3 nm of gold. Images were collected by detecting secondary electrons at a resolution of 2048 × 2288 pixels.

Atomic Force Microscopy (AFM) Characterization. AFM images were taken with a Park NX10 instrument (Park Systems Corp., Suwon, Korea), equipped with SmartScan software version 1.0 RTM 12d. All measurements were performed in an acoustic enclosure (JPK Instruments AG, Berlin, Germany) equipped with an antivibration table (e-Stable mini, Kurashicki Kako Co., LTD, Okayama, Japan). TAP300AL-G (Budget Sensors, Sofia, Bulgaria) tips with a declared tip radius of less than 10 nm were used for all measurements. No tip deconvolution was applied to the images, inducing a systematic error in the XY plane size definition, which is highly dependent on the exact tip shape and size.[42] Tip spring constants and instrument sensitivity were measured after each tip was mounted following the Sader and the tip displacement methods, respectively.[45,46] All images were taken in amplitude modulation mode (AM-AFM)[28] with a selected frequency below the resonance of the cantilever. Within this mode, the tip oscillates at a fixed frequency similar to the natural oscillations of the cantilever. The instrument records the amplitude oscillation and frequency shift of the oscillations as the tip interacts with the sample.[44] Based on the long-range interactions between the tip and the sample, both localized amplitude and localized frequency shifts are used to compose two datasets. These two channels can be used to extract information on the composition of the sample. Imaging parameters were kept constant with a free oscillation amplitude of 770 ± 28 nm, a set point of 250 ± 85 nm, an integral gain of 0.4 ± 0.3 A.U., a proportional gain of 0.3 ± 0.2 A.U., and a scanning rate of 0.4 ± 0.05 Hz. Imaging pixels were kept to 1024 × 1024 pixels, independently of the scan size. This allows for 48 nm/px in 50 μm images and 4.8 nm/px in 5 μm resolution. Height images were leveled by mean plane subtraction to remove tilt in the sample followed by a first-order polynomial baseline removal of each fast scan line independently. To remove bowing artifacts from the height channel, a second-order polynomial baseline removal followed, first along the slow scan direction and then along the fast scan direction. Forward and backward height signals were then averaged, giving the resulting height images. Phase channels were treated by mean plane subtraction to remove tilt followed by first-order polynomial baseline removal of each fast scan line independently. No further treatment was applied. The look up table (LUT) was adjusted to increase contrast of image features. The raw data was elaborated with the use of Gwyddion software (Version 2.54, GNU licensing). All data were treated in the same way to maximize comparison between datasets.

Confocal Laser Scanning Microscopy Analysis (cLSM). The biological response of cells grown on the collagen gels was visualized by cLSM (Zeiss LSM 710 meta, Germany). Briefly, the samples were washed three times with PBS and fixed with a 4 vol % solution of paraformaldehyde in PBS for 15 min. After three additional washes with PBS, samples were incubated with the rabbit monoclonal anti-Paxillin antibody (1:100 dilution in PBS) overnight at 4 °C followed by incubation with the goat anti-rabbit secondary antibody (IgG (H+L), Alexa Fluor 647, 1:100 dilution in PBS) for 2 h for paxillin visualization. F-actin cytoskeleton and the nuclei of the cells were stained with Alexa Fluor 488 Phalloidin (1:80 dilution in PBS) for 1 h and DAPI (1:100 dilution in PBS) for 5 min, respectively. Finally, the samples were washed three times with PBS and stored in 1 mL of PBS at 4 °C for further analysis. Samples were excited sequentially using 405 and 488 nm continuous lasers (at a magnification of 20X), and fluorescence was collected using DAPI and Alexa Fluor 488 emission filter at a resolution of 1024 and 1024 pixels.

Fluorescence-Enhanced Dark Field Microscopy. Collagen samples deposited on glass microscopy slides (Thermo Scientific SuperFrost Plus Adhesion slides, USA) and dried overnight were visualized using a 100× objective lens and a numerical aperture of 0.8 in a Cytoviva dual mode fluorescence-enhanced dark field microscopy setup (Cytoviva Inc., Auburn, AL, USA).

Image Analysis. Image analysis of cLSM data was performed using Fiji (NIH, US). The processing steps involve (i) intensity

https://doi.org/10.1021/acsabm.1c00844
ACS Appl. Bio Mater. 2021, 4, 8316−8324

thresholding to discard bias signal followed by binarization (Otsu's method)[47] and (ii) calculation of the pixel area of single cells, including major axis and minor axis values. Cell elongation from 80 individual cell data was determined by dividing the corresponding major axis and minor axis of the cytoskeleton area. Additionally, the cell spreading area corresponding to the pixel area was determined from 50 different individual cells.

Statistical Analysis. All statistical analyses were performed using GraphPad PRISM software (US). Rheology, LDH activity, cell area spreading, and cell elongation were analyzed using a one-way analysis of variance (ANOVA). Significance for all statistical analyses was defined as $p < 0.05$. All values are reported as the mean ± standard deviation of the mean for the independent biological triplicates.

■ ASSOCIATED CONTENT

Supporting Information

The Supporting Information is available free of charge at https://pubs.acs.org/doi/10.1021/acsabm.1c00844.

Time oscillation and frequency sweep rheological experiments of bare and composite collagen networks in Figure S1; experimental details of nanomaterial characterization by TEM and image analysis in Figure S2; AFM phase images of 40Au-Collagen and 15CNTs-Collagen Figure S3; SEM micrographs and cLSM low-magnification images of NIH-3T3 cells after 24 h of cultivation in hydrogel and bare collagen in Figure S4; cLSM images of stained F-actin, nuclei, and focal adhesion of NIH-3T3 fibroblasts cultured on the fabricated gels; graph showing the size of the focal adhesions calculated by image analysis in Figure S5; normalized TGF-β1 values in Figure S6; dimensions of the microfluidic device in Figure S7 (PDF)

■ AUTHOR INFORMATION

Corresponding Author

Alke Petri-Fink − *Adolphe Merkle Institute, Université de Fribourg, 1700 Fribourg, Switzerland; Department of Chemistry, University of Fribourg, 1700 Fribourg, Switzerland;* orcid.org/0000-0003-3952-7849; Email: alke.fink@unifr.ch

Authors

Giovanni Spiaggia − *Adolphe Merkle Institute, Université de Fribourg, 1700 Fribourg, Switzerland;* orcid.org/0000-0001-5668-7217

Patricia Taladriz-Blanco − *Adolphe Merkle Institute, Université de Fribourg, 1700 Fribourg, Switzerland;* Present Address: International Iberian Nanotechnology Laboratory (INL), Water Quality Group, Av. Mestre José Veiga s/n, 4715−330 Braga, Portugal

Dedy Septiadi − *Adolphe Merkle Institute, Université de Fribourg, 1700 Fribourg, Switzerland;* orcid.org/0000-0003-2353-7508

Roberto Diego Ortuso − *Adolphe Merkle Institute, Université de Fribourg, 1700 Fribourg, Switzerland*

Aaron Lee − *Adolphe Merkle Institute, Université de Fribourg, 1700 Fribourg, Switzerland*

Veronique Trappe − *Department of Physics, University of Fribourg, 1700 Fribourg, Switzerland*

Barbara Rothen-Rutishauser − *Adolphe Merkle Institute, Université de Fribourg, 1700 Fribourg, Switzerland;* orcid.org/0000-0002-7805-9366

Complete contact information is available at: https://pubs.acs.org/10.1021/acsabm.1c00844

Author Contributions

G.S. was responsible for the preparation and characterization of the hydrogels, taking the Cytoviva images, and all the cell experiments. P.T.-B. was responsible for writing the manuscript, the microfluidic design, and supervising hydrogel preparation and characterization. D.S. was responsible for supervising the cell experiments. R.D.O. was responsible for the AFM measurements. A.L. contributed to the scientific discussion. V.T. supervised the rheology experiments and data. A.P-F. and B.R.-R. were responsible for editing and the project principal investigators. All the authors have read and agreed to the published version of the manuscript.

Funding

The authors gratefully acknowledge financial support from the Swiss National Science Foundation (SNSF) through the Partnerships for International Research and Education (PIRE) program under grant number IZPIP0_177995, the Adolphe Merkle Foundation, and the University of Fribourg.

Notes

The authors declare no competing financial interest.

■ ACKNOWLEDGMENTS

The authors thank Dr. Sara Abalde-Cela from the International Iberian Nanotechnology Laboratory (INL, Braga, Portugal) for manufacturing the silicon master mold with the microfluidic pattern and Shuiling Chu for her assistance during the LDH assay.

■ REFERENCES

(1) Pawelec, K. M.; Best, S. M.; Cameron, R. E. Collagen: A Network for Regenerative Medicine. *J. Mater. Chem. B* **2016**, *4*, 6484−6496.

(2) Beckett, L. E.; Lewis, J. T.; Tonge, T. K.; Korley, L. T. J. Enhancement of the Mechanical Properties of Hydrogels with Continuous Fibrous Reinforcement. *ACS Biomater. Sci. Eng.* **2020**, *6*, 5453−5473.

(3) Dong, C.; Lv, Y. Application of Collagen Scaffold in Tissue Engineering: Recent Advances and New Perspectives. *Polymer* **2016**, 42.

(4) Taufalele, P. V.; VanderBurgh, J. A.; Muñoz, A.; Zanotelli, M. R.; Reinhart-King, C. A. Fiber Alignment Drives Changes in Architectural and Mechanical Features in Collagen Matrices. *PLoS One* **2019**, *14*, No. e0216537.

(5) Chaudhuri, O.; Cooper-White, J.; Janmey, P. A.; Mooney, D. J.; Shenoy, V. B. Effects of Extracellular Matrix Viscoelasticity on Cellular Behaviour. *Nature* **2020**, *584*, 535−546.

(6) Chen, X.; Fu, X.; Shi, J.; Wang, H. Regulation of the Osteogenesis of Pre-Osteoblasts by Spatial Arrangement of Electrospun Nanofibers in Two- and Three-Dimensional Environments. *Nanomedicine Nanotechnology, Biol. Med.* **2013**, *9*, 1283−1292.

(7) Jansen, K. A.; Licup, A. J.; Sharma, A.; Rens, R.; MacKintosh, F. C.; Koenderink, G. H. The Role of Network Architecture in Collagen Mechanics. *Biophys. J.* **2018**, *114*, 2665−2678.

(8) Smithmyer, M. E.; Sawicki, L. A.; Kloxin, A. M. Hydrogel Scaffolds as in Vitro Models to Study Fibroblast Activation in Wound Healing and Disease. *Biomater. Sci.* **2014**, *2*, 634−650.

(9) Dewle, A.; Pathak, N.; Rakshasmare, P.; Srivastava, A. Multifarious Fabrication Approaches of Producing Aligned Collagen Scaffolds for Tissue Engineering Applications. *ACS Biomater. Sci. Eng.* **2020**, *6*, 779−797.

(10) Laranjeira, M.; Domingues, R. M. A.; Costa-Almeida, R.; Reis, R. L.; Gomes, M. E. 3D Mimicry of Native-Tissue-Fiber Architecture

Guides Tendon-Derived Cells and Adipose Stem Cells into Artificial Tendon Constructs. *Small* **2017**, *13*, 1700689.
(11) Matthews, J. A.; Wnek, G. E.; Simpson, D. G.; Bowlin, G. L. Electrospinning of Collagen Nanofibers. *Biomacromolecules* **2002**, *3*, 232−238.
(12) Torbet, J.; Ronziére, M. C. Magnetic Alignment of Collagen during Self-Assembly. *Biochem. J.* **1984**, *219*, 1057−1059.
(13) Lee, P.; Lin, R.; Moon J, L. L. Microfluidic Alignment of Collagen Fibers for in Vitro Cell Culture. *Biomed. Microdevices* **2006**, *8*, 35.
(14) Haynl, C.; Hofmann, E.; Pawar, K.; Förster, S.; Scheibel, T. Microfluidics-Produced Collagen Fibers Show Extraordinary Mechanical Properties. *Nano Lett.* **2016**, *16*, 5917−5922.
(15) Wei, D.; Sun, J.; Yang, Y.; Wu, C.; Chen, S.; Guo, Z.; Fan, H.; Zhang, X. Cell Alignment Guided by Nano/Micro Oriented Collagen Fibers and the Synergistic Vascularization for Nervous Cell Functional Expression. *Mater. Today Chem.* **2018**, *8*, 85−95.
(16) Köster, S.; Leach, J. B.; Struth, B.; Pfohl, T.; Wong, J. Y. Visualization of Flow-Aligned Type I Collagen Self-Assembly in Tunable PH Gradients. *Langmuir* **2007**, *23*, 357−359.
(17) Nerger, B. A.; Brun, P.-T.; Nelson, C. M. Microextrusion Printing Cell-Laden Networks of Type I Collagen with Patterned Fiber Alignment and Geometry. *Soft Matter* **2019**, *15*, 5728−5738.
(18) Whitesides, G. M. The Origins and the Future of Microfluidics. *Nature* **2006**, *442*, 368−373.
(19) Daniele, M. A.; Boyd, D. A.; Adams, A. A.; Ligler, F. S. Microfluidic Strategies for Design and Assembly of Microfibers and Nanofibers with Tissue Engineering and Regenerative Medicine Applications. *Adv. Healthcare Mater.* **2015**, *4*, 11−28.
(20) Saeidi, N.; Sander, E. A.; Ruberti, J. W. Dynamic shear-influenced collagen self-assembly. *Biomaterials* **2009**, *30*, 6581−6592.
(21) Ashokkumar, M.; Ajayan, P. M. Materials Science Perspective of Multifunctional Materials Derived from Collagen. *Int. Mater. Rev.* **2021**, *66*, 160−187.
(22) MacDonald, R. A.; Laurenzi, B. F.; Viswanathan, G.; Ajayan, P. M.; Stegemann, J. P. Collagen−Carbon Nanotube Composite Materials as Scaffolds in Tissue Engineering. *J. Biomed. Mater. Res. Part A* **2005**, *74A*, 489−496.
(23) Homenick, C. M.; Sheardown, H.; Adronov, A. Reinforcement of Collagen with Covalently-Functionalized Single-Walled Carbon Nanotube Crosslinkers. *J. Mater. Chem.* **2010**, *20*, 2887−2894.
(24) Kim, T.; Sridharan, I.; Zhu, B.; Orgel, J.; Wang, R. Effect of CNT on Collagen Fiber Structure, Stiffness Assembly Kinetics and Stem Cell Differentiation. *Mater. Sci. Eng. C* **2015**, *49*, 281−289.
(25) Xing, R.; Liu, K.; Jiao, T.; Zhang, N.; Ma, K.; Zhang, R.; Zou, Q.; Ma, G.; Yan, X. An Injectable Self-Assembling Collagen−Gold Hybrid Hydrogel for Combinatorial Antitumor Photothermal/Photodynamic Therapy. *Adv. Mater.* **2016**, *28*, 3669−3676.
(26) Yang, Y.; Wang, K.; Gu, X.; Leong, K. W. Biophysical Regulation of Cell Behavior—Cross Talk between Substrate Stiffness and Nanotopography. *Engineering* **2017**, *3*, 36−54.
(27) Rogers, T. G. Rheological Characterization of Anisotropic Materials. *Composites* **1989**, *20*, 21−27.
(28) Stark, M.; Möller, C.; Müller, D. J.; Guckenberger, R. From Images to Interactions: High-Resolution Phase Imaging in Tapping-Mode Atomic Force Microscopy. *Biophys. J.* **2001**, *80*, 3009−3018.
(29) Voigtländer, B. *Scanning Probe Microscopy*, 1st ed.; Springer, Berlin, Heidelberg, DOI: 10.1007/978-3-662-45240-0.
(30) Mensah, B.; Kim, H. G.; Lee, J.-H.; Arepalli, S.; Nah, C. Carbon Nanotube-Reinforced Elastomeric Nanocomposites: A Review. *Int. J. Smart Nano Mater.* **2015**, *6*, 211−238.
(31) Kumar, K.; Sul, O.; Strauf, S.; Choi, D. S.; Fisher, F.; Prasad, M. G.; Yang, E.-H. A Study on Carbon-Nanotube Local Oxidation Lithography Using an Atomic Force Microscope. *IEEE Trans. Nanotechnol.* **2011**, *10*, 849−854.
(32) Califano, J. P.; Reinhart-King, C. A. Substrate Stiffness and Cell Area Predict Cellular Traction Stresses in Single Cells and Cells in Contact. *Cell. Mol. Bioeng.* **2010**, *3*, 68−75.
(33) Zemel, A.; Rehfeldt, F.; Brown, A. E. X.; Discher, D. E.; Safran, S. A. Cell shape, spreading symmetry and the polarization of stress-fibers in cells. *J Phys Condens Matter* **2010**, *22*, 194110−194110.
(34) Zhong, J.; Yang, Y.; Liao, L.; Zhang, C. Matrix Stiffness-Regulated Cellular Functions under Different Dimensionalities. *Biomater. Sci.* **2020**, *8*, 2734−2755.
(35) Negmadjanov, U.; Godic, Z.; Rizvi, F.; Emelyanova, L.; Ross, G.; Richards, J.; Holmuhamedov, E. L.; Jahangir, A. TGF-B1-Mediated Differentiation of Fibroblasts Is Associated with Increased Mitochondrial Content and Cellular Respiration. *PLoS One* **2015**, *10*, e0123046−e0123046.
(36) Gilbert, R.; Vickaryous, M.; Viloria-Petit, A. Signalling by Transforming Growth Factor Beta Isoforms in Wound Healing and Tissue Regeneration. *J. Dev. Biol.* **2016**, 21.
(37) ABRAHAMIAN, A.; Xi, M.-S.; Donnelly, J. J.; Rockey, J. H. Effect of Interferon-γ on the Expression of Transforming Growth Factor-β by Human Corneal Fibroblasts: Role in Corneal Immunoseclusion. *J. Interferon Cytokine Res.* **1995**, *15*, 323−330.
(38) Hinz, B. The Extracellular Matrix and Transforming Growth Factor-B1: Tale of a Strained Relationship. *Matrix Biol.* **2015**, *47*, 54−65.
(39) Mih, J. D.; Marinkovic, A.; Liu, F.; Sharif, A. S.; Tschumperlin, D. J. Matrix Stiffness Reverses the Effect of Actomyosin Tension on Cell Proliferation. *J. Cell Sci.* **2012**, *125*, 5974−LP − 5983.
(40) Clark, R. A. F.; McCoy, G. A.; Folkvord, J. M.; McPherson, J. M. TGF-β1 stimulates cultured human fibroblasts to proliferate and produce tissue-like fibroplasia: A fibronectin matrix-dependent event. *J. Cell. Physiol.* **1997**, *170*, 69−80.
(41) Kievit, F. M.; Cooper, A.; Jana, S.; Leung, M. C.; Wang, K.; Edmondson, D.; Wood, D.; Lee, J. S. H.; Ellenbogen, R. G.; Zhang, M. Aligned Chitosan-Polycaprolactone Polyblend Nanofibers Promote the Migration of Glioblastoma Cells. *Adv. Healthcare Mater.* **2013**, *2*, 1651−1659.
(42) Prager-Khoutorsky, M.; Lichtenstein, A.; Krishnan, R.; Rajendran, K.; Mayo, A.; Kam, Z.; Geiger, B.; Bershadsky, A. D. Fibroblast Polarization Is a Matrix-Rigidity-Dependent Process Controlled by Focal Adhesion Mechanosensing. *Nat. Cell Biol.* **2011**, *13*, 1457−1465.
(43) Enüstün, B. V.; Turkevich, J. Coagulation of Colloidal Gold. *J. Am. Chem. Soc.* **1963**, *85*, 3317.
(44) Markiewicz, P.; Goh, M. C. Simulation of Atomic Force Microscope Tip−Sample/Sample−Tip Reconstruction. *J. Vac. Sci. Technol. B Microelectron. Nanom. Struct. Process. Meas. Phenom.* **1995**, *13*, 1115−1118.
(45) Sader, J. E.; Chon, J. W. M.; Mulvaney, P. Calibration of Rectangular Atomic Force Microscope Cantilevers. *Rev. Sci. Instrum.* **1999**, *70*, 3967−3969.
(46) Hutter, J. L.; Bechhoefer, J. Calibration of Atomic-force Microscope Tips. *Rev. Sci. Instrum.* **1993**, *64*, 1868−1873.
(47) Xu, X.; Xu, S.; Jin, L.; Song, E. Characteristic Analysis of Otsu Threshold and Its Applications. *Pattern Recognit. Lett.* **2011**, *32*, 956−961.

https://doi.org/10.1021/acsabm.1c00844
ACS Appl. Bio Mater. 2021, 4, 8316−8324